T13 - Instrumentation

T13 - P221

THE STUDSVIK NEUTRON RESEARCH LABORATORY

S.-G. Eriksson[a,b], A. Ahi[b], A.K. Azad[a,b], J. Eriksen[a], S.A. Ivanov[a,c], A. Rennie[a], A. Mellergård[a], H. Rundlöf[a], M. Valkeeapää[b] and P. Zetterström[a]

[a]Studsvik Neutron Research Laboratory, Uppsala University, 611 82 Nyköping, Sweden; [b]Dept. of Inorganic Chemistry, University of Gothenburg, 412 96 Göteborg, Sweden; Sweden, [c]Karpov Institute of Physical Chemistry, 103064 Moscow, Russia.

The Studsvik Neutron Research Laboratory (NFL) is the Swedish centre for research using neutrons in physics, chemistry, metallurgy, and materials science. NFL is centred round the 50 MW R2 reactor, which is of swimming pool type, and can be classed as a medium flux reactor for neutron scattering applications. The facility includes a range of neutron scattering instruments with an emphasis on diffraction applications, including single crystal diffraction, powder diffraction, diffraction from liquids and amorphous materials, and residual stress and texture diffraction. Information from the total scattering – that is the Bragg scattering as well as the diffuse scattering – is taken into account when extracting structural information from the data. Average structure as well as local structure can be handled

It should be emphasised that activities at Studsvik today cover the full chain "Chemical synthesis – Neutron scattering – Modelling". A very strong feedback between the different links in the chain is one of the key factors behind the rapid development of the laboratory. Relevant scientific examples will be highlighted in order to illustrate work being carried out. Furthermore, NFL´s goals and its expected role within the Swedish and the European scientific community, will briefly be discussed.

T13 - P222

R2D2: A NEW NEUTRON POWDER DIFFRACTOMETER AT NFL

A. Wannberg, M. Grönros, A. Mellergård, L-E. Karlsson, R. G. Delaplane[1], B. Lebech[2]

[1]Studsvik Neutron Research Laboratory, Uppsala University, 611 82 Nyköping, Sweden
[2]Risø National Laboratory, Materials Research Department, DK-4000 Roskilde, Denmark

The powder diffractometer transferred from Risø (formerly named TAS3) has been installed at NFL (Studsvik, Sweden) and is now in operation. As the second powder diffractometer on the R2 reactor it has been named R2D2. It is installed on the 'tangential' beam tube H9; the incident wavelength is 1.55 Å, using a vertically focusing Ge(511) monochromator crystal with a take-off angle of 90°. The instrument has a bank of twenty ^{3}He detectors mounted behind twenty 10' Soller collimators. A complete powder diffraction pattern is obtained with a 5° scan. Projects making use of this instrument include complex metal hydrides, magnetic materials, complex metal oxides such as perovskites and nano-structured materials. Effective use of R2D2 has been demonstrated together with *in situ* experiments performed on SLAD, a high intensity, low resolution instrument. A sample undergoing changes in structure as a function of temperature or pressure can be monitored on SLAD and then transferred to R2D2 when a new phase develops and higher resolution is needed.

This facility is now open for use by the international user community.

T13 - P223

NEUTRON RTOF DIFFRACTOMETER FSD FOR RESIDUAL STRESS INVESTIGATION

G. D. Bokuchava, A. V. Tamonov, V. V. Sumin, A. M. Balagurov

Frank Laboratory of Neutron Physics, Dubna, Russia, FLNP JINR, Joliot Curie str, 6, Dubna, Moscow reg, 141980, RUSSIA tamonov@nf.jinr.ru

FSD – it's high resolution Fourier Stress Diffractometer.

FSD is a neutron reverse time-of-flight Fourier diffractometer intended for precise residual stress investigations in bulk samples and advanced materials. FSD diffractometer combines a high neutron flux at sample position, ~2*10^6 n/cm^2/s, provided by the IBR-2 high flux pulsed reactor (FLNP, Dubna, Russia), and a high resolution over a wide range of *d*-spacings. All experimental facilities of IBR-2 are open to the general scientific community. The User Guide for neutron experimental facilities at FLNP and Guide for sample environment experimental equipment on the IBR-2 spectrometers is available by request.

FSD was constructed in the frame of cooperation between FLNP JINR (Dubna) and PNPI (Gatchina). The main specific feature of FSD distinguishing it from other Fourier-diffractometers operating at steady state reactors, is the capability of analysis of triple correlations of signals from the neutron source, Fourier-chopper and the detector. As a result, the neutron intensity measured with FSD is:

$$I(t) \sim R_s(t-t)R_c(t-t)s(t)dt + c\, R_s(t-t)s(t)dt + B(t),$$

where R_c is the resolution function of the Fourier chopper, R_s is the source pulse, s is the scattering cross section of the sample, B is the conventional background, and c is a certain constant close to 1. The second term, called "the correlation background", is proportional not to the total detected intensity, as in the case of steady state reactors, but to the intensity measured in short time intervals equal to the width of the source pulse (~350 s for IBR-2). This leads to a substantial decrease of the correlation background, better quality of diffraction patterns, and permits the useful wavelength interval to be extended.

This work was supported by RFBR grant ą 04-02-97249.

[1] http://nfdfn.jinr.ru/proposals.html

[2] http://nfdfn.jinr.ru/fks/fsd.html

[3] G.D. Bokuchava, V.L. Aksenov, A.M. Balagurov, V.V. Zhuravlev, E.S. Kuzmin, A.P. Bulkin, V.A. Kudryashev, V.A. Trounov "Neutron Fourier diffractometer FSD for internal stress analysis: first results", Applied Physics A: Materials Science & Processing, 2002, v.75.

T13 - P224

BENT PERFECT CRYSTAL (BPC) MONOCHROMATOR AT THE MONOCHROMATIC FOCUSING CONDITION

Y. N. Choi[1], S. A. Kim[1], S. K. Kim[1], S. B. Kim[1], C. H. Lee[1], P. Mikula[2], M. Vrána[2]

[1]HANARO Centre, Korea Atomic Energy Research Institute, Yuseong, Daejeon 305-600, Korea
[2] Nuclear Physics Institute and Research Centre Řež, Ltd., 25068 Řež near Prague, Czech Republic.

Conventional neutron diffractometers employing a single mosaic monochromators are oerated only in the parallel (+,-) measurement setting, because the resolution property of the anti-parallel (+,+) setting is much worse [1]. However, if we could use the both setting with the equivalent resolution, the measurement efficiency could be twice of that related to the traditional measurement mode. A strong difference in the resolution properties in the parallel and antiparallel settings is brought about by a nonnegligible correlation of the monochromatized beam impinging the sample in the scattering plane. In order to overcome this problem the momentum distribution of the monochromatized neutrons should be symmetric with respect to the axis of the beam impinging the sample. Three monochromator arrangements which could provide a rather highly collimated monochromatic neutron beam with a negligible correlation with a reasonable keeping the luminosity and the instrument resolution on an acceptable level) have been already tested, namely:

1. Fully asymmetric diffraction (FAD) geometry of the Si-BPC monochromator [2-4]. The FAD geometry of the monochromator is in fact a limiting case of the Fankuchen geometry which implicates some limitations on a choice of the crystal. At present, a bent perfect Si-crystal with a very low attenuation for neutrons could be the best candidate for this purpose. According to our information, the FAD geometry of the monochromator has not been employed for a routine work, though some tests of the FAD monochromator systems have been already carried out [2-4].

2. Dispersive double-crystal setting [5-8]. A strongly dispersive double-crystal arrangement of two mosaic or bent perfect crystals or combination of them is another monochromator performance having a negligible correlation of the monochromatic neutrons in the scattering plane but providing a sufficient neutron current at the sam-

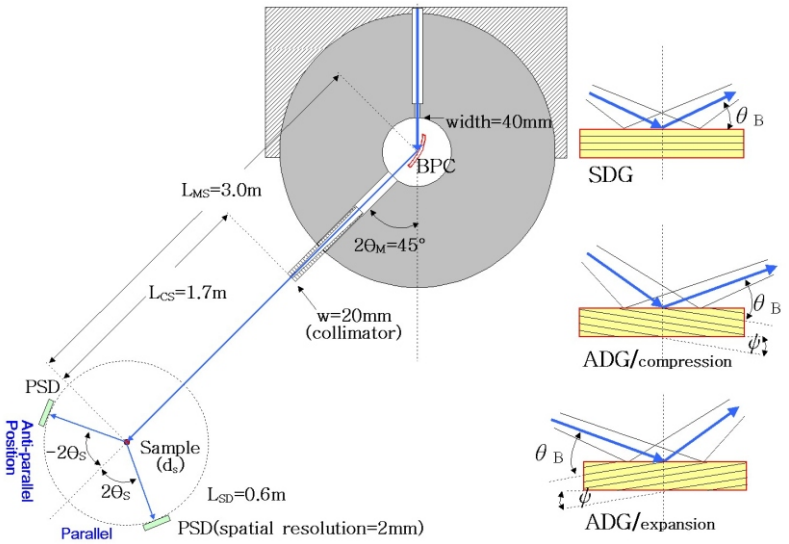

Fig. 1. Experimental set-up at ST1 beam port of the HANARO reactor and three diffraction geometries used in the test.

ple position represents. The strongly dispersive double crystal setting can be achieved either by using two crystals with the same lattice constant mutually in the antiparallel (+,+) arrangement or by using two crystals with a large difference in the lattice constants.

3. Multiple reflection *Umweganregung* monochromator [7-10]. *Umweganregung* monochromator is based on a multiple Bragg diffraction process (often referred to as simultaneous reflections) realised in one crystal and can be observed when a crystal lattice is oriented in such a way that more than one set of planes are simultaneously operative for a given wavelength. In the extreme case the *Umweganregung* effect going through a secondary and tertiary reflection can simulate forbidden primary reflection [11-13]. It has been already demonstrated [7, 9, 10] that strong multiple reflection effects resulting in *Umweganregung* and observed in elastically deformed perfect crystals can be used for ultra-high monochromatization and diffraction studies.

This contribution deals with another performance of the BPC monochromator adjusted for the monochromatic focusing. Contrary the above mentioned monochromator performances where a narrow (negligible -distribution) phase-space element with a reasonable is aligned parallely to the beam axis, in this case a narrow phase-space element with quite a large -distribution but small -distribution is aligned perpendicularly to the beam axis. As will be shown, the BPC monochromator at monochromatic focusing condition can provide equal resolution property at both (+,-) as well as (+,+) settings and gives a chance to use both sides of the scattering half-plane. Three diffraction geometries (symmetric, asymmetric with the diffracted beam compression and asymmetric with the diffracted beam expansion) with BPC monochromators were tested. As schematically shown in Fig. 1, three typical diffraction geometries were chosen to investigate the dependence of the *FWHM* of the line profiles and the resolution the corresponding (*d/d*)-resolution (the (*d/d*)- data were calculated from the *FWHM*-data) on the monochromator bending radius. For the SDG-experiment, a Si(220) crystal slab of the dimensions of 200x30x3 mm^3 was used. For the ADG/compression and ADG/expansion experiments, Si(211) crystal slab (thickness of 3.8 mm) with 311 planes at =10° and a special cut of silicon slab (thickness of 3.8 mm) with the planes (311) at =20 , respectively, were used. The calculated values of the bending radii R_{MF} corresponding to individual geometries are 7.84 m, 13.9 m and 4.46 m, respectively. Figs. 2-4 display the experimental results obtained with three different monochromator crystals and demonstrate that when R approaches to R_{MF}, the resolution property becomes equivalent in both diffraction geometries.

In principle, the measurement efficiency in powder diffractometry could be increased twice and the range of scattering angles could be substantially extended. In the case of the strain measurements the monochromatic focusing performance permits a measurement of two strain com-

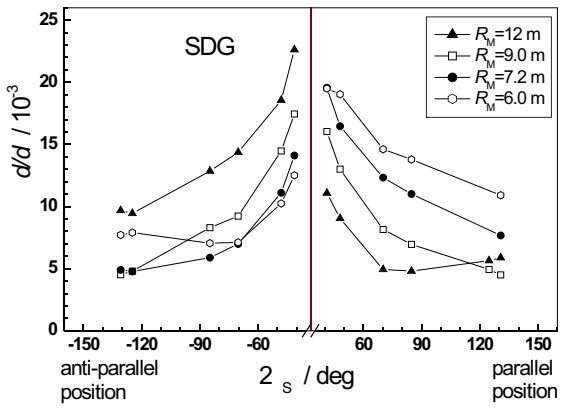

Fig. 2. Experimental data of *d/d* resolution for Si(220) (= 0.147 nm) crystal slab set in symmetric diffraction geometry (=22.5°, R_{MF}= 7.84 m).

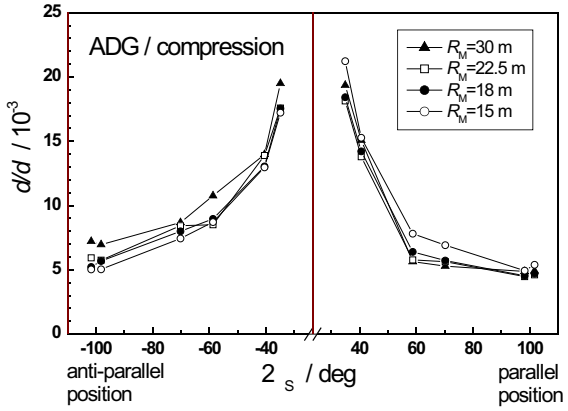

Fig. 3. Experimental data of *d/d* resolution for Si(311) (=0.125 nm) crystal slab set in asymmetric diffraction geometry with the out beam compression (=12.5°, R_{MF}= 13.9 m).

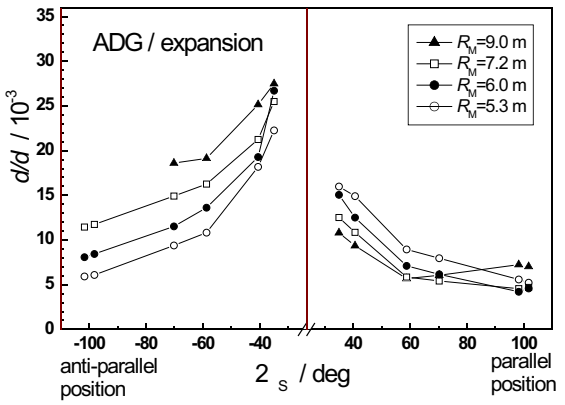

Fig. 4. Experimental data of *d/d* resolution for Si(311) (=0.125 nm) crystal slab set in asymmetric diffraction geometry with the out beam expansion (=42.5°, R_{MF}= 4.46 m).

ponents simultaneously. Another application of such focusing monochromator could be for inelastic scattering experiments on triple axis spectrometer. (*E/E*)-resolution is then determined by the lateral dimension of the sample and the effective mosaicity of the BPC monochromator which is about one order of magnitude smaller that the mosaicity of conventional mosaic monochromators. Of course, similarly to the BPC-monochromator, a BPC-analyser at the *monochromatic focusing* condition could also be used, though due to a generally smaller sample-analyser distance L_{SA} (L_{SA}<L_{MS}) the bending radius of the analyser R_{MF} is correspondingly smaller.

Acknowledgement
We are grateful to the in-house collaborators, Mr. B.H. Choi, Mr. Y.H. Choi, Mr. K.P. Hong, Dr. M.K. Moon and Dr. V.T. Em for the experimental preparations and to Ms. H.S. Oh for the numerous data processing. This work was in Korea supported by the Korean Ministry of Science and Technology through the National Nuclear R&D Programme and the Scientist Visiting Program and in the Czech Republic by the research projects GA-CR (No. 202/03/0891), GA-CAS (No. A1048003) and COST – OC P7.003 and MSM2672244501.

1. G. E. Bacon, Neutron Diffraction, Clarendon Press, Oxford (1975) pp.101-111.
2. P. Mikula, P. Lukáš and R. Michalec, J. Appl. Cryst. **20** (1987) 428-430.
3. P. Mikula, J. Kulda, L. Horalík, B. Chalupa and P. Lukáš, J. Appl. Cryst. **91** (1986) 324-330.
4. M.R. Muslih, I. Tanaka, P. Mikula, N. Niimura, JAERI Review 2002-028, p. 119.
5. P. Mikula et al., Mater. Sc. Forum, Vols. **404-407** (2002) 299-302.
6. M. Popovici and A.D. Stoica, Appl. Phys. A **74** (2002), S273-S276.
7. P. Mikula, M. Vrána, V. Wagner, Y. N. Choi, S. A. Kim, H. S. Oh, K. H. Sung and C. H. Lee, Proc. of Int. Conf. ATEM´03, Sept. 10-12, 2003, Nagoya, Japan. CD ROM Published by JSME No. 03-207, paper OS04W0288.
8. M. Vrána, P. Mikula, R.T. Michalec, J. Kulda and J. Vávra Acta Cryst. **A 37** (1981) 459-465.
9. P. Mikula, J. Kulda, M. Vrána, R.T. Michalec and J. Vávra, Nucl. Instrum. Methods, 197 (1982) 563-566.
10. P. Mikula et al., Proc. of the Symp. Neutron Scattering, August 6-8, 1984, West Berlin, HMI-B 411, p. 233-235.
11. M. Renninger, Z. Phys. **106** (1937) 141-176.
12. R.M. Moon and C.G. Shull, Acta Cryst. **17** (1964) 805-812.
13. Shih-Lin Chang, Multiple Diffraction of X-rays in Crystals, Springer Verlag, 1984; Moscow "Mir", 1987.

T13 - P225

NEW DETECTOR TECHNOLOGY FOR X-RAY DIFFRACTION

L. Brügemann[1], A. Kern[1], H.-G. Krane[1], R. Durst[2], B. He[2], Y. Diawara[2]

[1]Bruker AXS GmbH, Germany, [2]Bruker AXS Inc., USA

A new one-dimensional detector generation for X-ray diffraction based on the "MikroGap" technology will be introduced. This new technology is characterized by near-ideal quantum efficiency, high energy resolution, zero intrinsic noise and the highest local and global count rates perfectly matching X-ray diffraction requirements.

The detector is radiation-hard, maintenance-free, does not require gas purge and can be operated with all common laboratory X-ray sources including but not limited to Mo-, Cu-, Co-, and Cr-tubes. Its remarkable energy resolution makes this detector even suited for retained austenite measurements using Cu-radiation!

Due to its large active window of 50x16mm the detector is perfectly suited for operation in both scanning and fixed mode. Typical measurement times in scanning mode are < 5 minutes for an angular range from ~0° up to 160° 2 . In fixed mode measurement times down to 100 ms per ~12° 2Theta provide for e.g. non-ambient studies in real time.

This presentation will discuss the "Mikrogap" technology and resulting detector specifications. The performance of the new detector will be demonstrated using several examples with datasets acquired under ambient and non-ambient (temperature, temperature/relative humidity) conditions for structure analysis.

T13 - P226

X-RAY AND NEUTRON DIFFRACTION APPLICATIONS USING POLYCAPILLARY OPTICS

Thomasin C. Miller, Huapeng Huang, Walter Gibson

X-ray Optical Systems, Inc., 15 Tech Valley Drive, East Greenbush, NY 12061

Polycapillary x-ray optics have developed into an enabling technology for both x-ray and neutron diffraction measurements. These optics operate by collecting x-rays or neutrons and efficiently propagating them by total external reflection to form focused or parallel beams.

Polycapillary optics can be used to enhance x-ray diffraction applications. Some of the major drawbacks of traditional XRD are that it is often based on bulky equipment with high power requirements. Furthermore, most conventional instruments use a parafocusing Bragg-Brentano geometry, offering the advantages of high-resolution and high beam-intensity analysis at the cost of very precise alignment requirements and carefully prepared samples. These constraints are removed if the incident x-ray beam is parallel. In parallel beam x-ray diffraction, a capillary optic can be used to form an intense parallel x-ray excitation beam resulting in very high x-ray intensities at the sample surface. The parallel beam geometry eliminates errors associated with parafocusing geometry and does not require stringent sample preparation. Furthermore, through use of a polycapillary collimating optic, the target parallel beam XRD system can be combined with a low power x-ray source, reducing instrument size and power requirements. The development of compact, low-power, safe, stable, and reliable integrated source-optic combinations (X-BeamsÔ) greatly facilitates the use of x-ray diffraction in scientific or industrial settings where use of x-ray diffraction has heretofore been impractical. Process applications using collimating optics in a parallel geometry for phase distribution measurements in the pharmaceutical industry and thin film texture measurements for superconductor layers and magnetic films will be reviewed.

Polycapillary optics can also be used to enhance general purpose powder diffraction (GPPD) using neutrons. A major limitation of neutron diffraction measurement is the relatively low flux available from neutron sources. Such measurements often require large samples and long data collection times. Monolithic polycapillary optics were used to increase the neutron current density at the sample resulting in a greatly increased optic gain making it possible to measure diffraction from much smaller samples. Results from these studies will be reviewed.

T13 - P227

FAULTS, A NEW PROGRAM FOR REFINEMENT OF LAYERED STRUCTURES POWDER DIFFRACTION PATTERNS

M. Casas-Cabanas[1,2], J. Rodríguez-Carvajal[2], M. R. Palacín[1]

[1]Institut de Cičncia de Materials de Barcelona (CSIC), Campus UAB E-08193 Bellaterra, Catalonia, Spain
[2]Laboratoire Léon Brillouin, CEA CNRS, Saclay, FR-91191, Gif-sur-Ivette Cedex, France.

A new program for refinement of layered structures is herein presented. FAULTS is based in the Diffax program, developed by Treacy et al. [1], which simulates selected area electron diffraction and powder diffraction patterns (X-ray and neutrons) by means of a recursion algorithm that calculates the incoherent sum of diffracted intensities of any type of crystal system and particularly those containing planar defects.

In order to deal with the limitations of a simple simulation, refinement of all the parameters involved in the calculation of the diffracted intensities has been implemented in FAULTS, which can be carried out using a local optimisation algorithm, Nelder-Mead simplex [2], or global ones, as Simulated Annealing [3] or Multilevel Clustering [4, 5].

The refinable parameters are read by FAULTS from a free format input data file, similar to that of Diffax, where each value is associated to a refinement code that allows the possibility of restrictions. The parameter's high and low limits as well as the nature of the boundary conditions are provided by the user.

The experimental XRD or NPD patterns can be read from many different formats and background subtraction can be achieved by linear interpolation or polynomially after applying the scale factor.

Another major feature of FAULTS is the implementation of a more adequate isotropic size broadening treatment which takes into account the Gaussian (H_G) and Lorentzian (H_L) contributions to the FWHM in addition to the consideration of a finite number of layers per crystallite already present in Diffax. As these are refinable parameters, this treatment allows a successful description of the separate contributions to line broadening of instrumental features, the finite crystallite size and planar defects.

As an indicator of the adjustment's quality, agreement indices such as the R_P and R_{WP} values, or ^{2}, are calculated at the end of each refinement cycle.

At present the program is thoroughly being tested so as to detect possible errors, determine the optimal strategies for the refinement process and to try to speed up the calculations. Also the addition of new features considering other

aspects of the diffraction problem is currently being performed. The structure and operation of the program as well as some examples will be shown.

Aknowledgements
This work was supported by the CSIC (I3P program) and the Departament d'Universitats, Recerca i Societat de la Informació de la Generalitat de Catalunya.

[1] M.M. Treacy, J.M. Newsam, M.W. Deem, *Proc. R. Soc. London Ser. A,* 433 (1991), 499-520.

[2] J.A. Nelder, R. Mead, *The computer journal,* 7 (1965) 308-313.

[3] S. Kirkpatrick, C. D. Gelatt, Jr., M. P. Vecchi, *Science*, 220 (1983) 671-680.

[4] Boender, C.G.E., A.H.G. Rinnooy Kan, G.T. Timmer, L. Stougie, *Mathematical Programming* 22(1982) 125-140.

[5] Csendes, T., *Acta Cybernetica*, 8(1988) 361-370.

T13 - P228

PROGRAM PACKAGE FOR POWDER STRUCTURAL REFINEMENT

V. A. Firsova, V. S. Fundamensky, N. G. Pyatygina

St.-Petersburg, Bourevestnik Inc., fundamensky@crystal.pu.ru

Two new programs are included into the program package PDWin. The first program is developed for the modeling theoretical diffraction patterns using a known structure. Prior information may include the data on various optic schemes of device. The second program is developed for the Rietveld refinement of single and multiphase samples.

The program THEORPATTERN allows to calculate the integrated intensities for single and multiphase samples with the given weight ratios of phases. The results can be represented as plots, tables and files suitable for the further analysis. The input data include the information on the unit cell parameters, space group in the standard or user settings, and on chemical composition for each phase. Besides, the manual input of atomic parameters is provided that allows editing the information on the coordinates, isotropic or anisotropic thermal parameters of atoms and the occupancies of their positions. The program automatically takes into account the anomalous dispersion of atoms and their ionized states. The program can import files *.par (CSD), *.ins (SHELX) or CIF.

The user can input the information on the method of data collection and angular interval, the characteristics of the hypothetical device and on the radiation spectrum. For example, a diffraction pattern can be plotted for various angular resolutions of the device, goniometer radii, sample thickness, and for zero angles of the detector, etc. Texture for each phase can be taken into account. Diffraction pattern can be presented as a bar – diagram, and the peak profiles are simulated by pseudo-Voigt function either for K_1 line or $K_1 + K_2$, doublet, or by a doublet instrumental function.

It is possible to calculate a pattern of a specified phase or a summarized pattern of any combination of the phases chosen by the user. The chosen resolution defines a degree of overlapped peaks. The output tables contain the information on integrated and maximal intensities of completely resolved peaks and on the corresponding intensities of the overlapped peaks accounting for the given angular resolution.

The program for Rietveld refinement allows the use of single or multiphase samples using the measured powder diffraction pattern. The input and editing procedures of atomic parameters and other data on each phase do not differ basically from those described above. The experimental data can be input from the data files measured on the autodiffractometers DRON-4, DRON-6, DRON-7 or from ASCII files containing the information on intensity and 2 (d) measured in any other powder diffractometer. The program allows to input the data on the measurement conditions.

There is an opportunity of input and further refinement of U, V, W, X and Y parameters, which define FWHM of the peaks approximated by Gaussian and Lorentzian functions, not only for different phases, but also for the reflections with different types of Miller indices for one and the same phase. Besides, the user can choose a Gauss/Lorentz ratio in pseudo-Voigt function and an asymmetry parameter for the initial approximation. Frequently during the refinement of profile parameters the problem of choosing the borders of a specified peak arises. Usually, 5-6 values of FWHM values are acceptable. However, it is well known, that the Gaussian function falls down much rapidly than the Lorentzian. Therefore, to reduce the calculation time, the opportunity of a separate choice of the widths of peaks bases for Gaussian and Lorentzian parts is provided.

The zero cycle of refinement includes the background refinement (background is approximated by a power polynomial with the power value chosen by a user), the refinement of the scale factor and the calculation of the phase weight ratios.

The refinement strategy is determined by the table with the refinement parameters, which can be chosen at any stage of the procedure. The weight non-linear method of the least squares (Marquardt method) is used for the refinement. The following parameters are accessible: a zero shift of the detector, unit cell dimensions,, atomic and thermal parameters, profile parameters, phase ratios and background polynomial coefficients. It is possible to use the damping factor to prevent a divergence a procedure.

Atomic parameters include coordinates and thermal (isotropic/anisotropic) parameters of atoms, occupation factors and texture parameters. Fixing of parameters and the special relations between positional and thermal parameters of the atoms in special positions are generated auto-

matically during the data input. The user can fix atomic parameters and introduce the relations between them at the stage of data input of each phase. At any stage of strategy choice it is possible to permit/forbid the refinement of all positional and/or all thermal parameters and/or all occupation factors whose values are permitted to refine during the input stage.

It is possible to permit/forbid the refinement of the profile parameters U, V, W, X, Y, a Gaussian/Lorentzian ratio and of the asymmetry parameter individually for each phase.

At any stage of the refinement it is possible to change its strategy based on intermediate results.

Both programs allow to calculate interatomic distances and angles, and torsion angles and equations of flat and linear structural fragments and the angles between them.

T13 - P229

X- RAY POWDER DIFFRACTION DATA OF SYNTHETIC ß- TRICALCIUM PHOSPHATE $Ca_3(PO_4)_2$

Ermrich, M.[1] and Peters, F.[2]

[1]Röntgenlabor Dr. Ermrich, Am Kandelborn 7, D-64354 Reinheim, Germany
[2]Curasan AG, In der Schildwacht 13, D-65933 Frankfurt/Main, Germany

The ß- Tricalcium Phospate $Ca_3(PO_4)_2$ has been established as an important bioceramic.

The Whitlockite mineral and its PDF data (PDF #9-169) are generally in use to identify the ß- TCP phase in practice. But, the lattice parameters of ß- TCP change with different Mg- contents. That makes the assignment using Search/Match programs sometimes difficult.

At the latest now, the synthesis of pure ß- TCP for the application as biomaterial succeeded. For that, only a very low amount of < 0,5 wt. % Mg is necessary to stabilise the structure as already given by the raw materials.

This synthetic ß- TCP with the lowest Mg- content was investigated by X-ray powder diffraction. After refinement the rhombohedral cell parameters (R-3c, 167) were determined to

a = 10.4183(5) Å
c = 37.3464(23) Å
V = 3510.52(47) $Å^3$
Z = 21
D_x = 3.081 g/cm^3.

T13 - P230

CALCULATING THE PEAK SHAPE OF AXIALLY FOCUSSING POWDER DIFFRACTOMETERS

Daniel M. Többens

Hahn-Meitner-Institut, Glienicker Straße 100, D-14109 Berlin, Germany

The accurate description of the shape of individual peaks is essential for high quality Rietveld refinements. Systematic errors of the peak shape reduce the precision of the refinement and can result in parameters refined to systematically wrong values. Due to the speed of modern computers pure numerical calculation of peak shapes has become feasible. Thus instrument geometries increasing the intensity can be chosen, even if more complicated peak shapes without good analytical description result. Pure numerical Monte-Carlo simulations show good results simulating instruments. However, they still take to long to be used in routine Rietveld refinement, where relevant parameters, i.e. sample height, can vary from one measurement to the next.

In neutron powder diffraction, axially focussing monochromators have become widely used. The geometry of these instruments (see figure) results in peak shapes for which a description by currently available non-MC models is not satisfying. The peak shape is mainly determined by the instrumental axial asymmetry function (AAF). A fundamental approach for calculating the AAF for this type of geometry is discussed in this paper. The various effects to

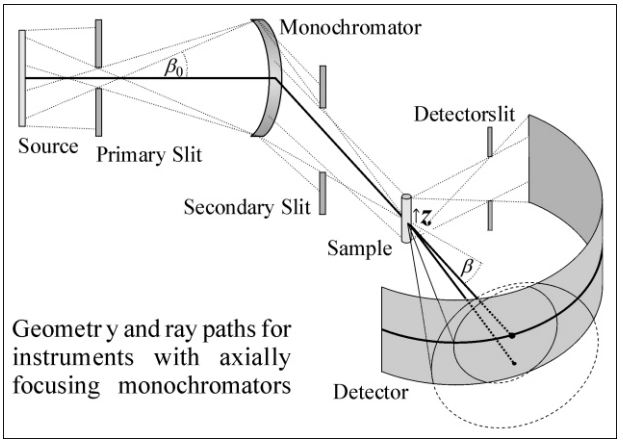

Geometr y and ray paths for instruments with axially focusing monochromators

be considered are explained in detail and a programme, QUASIMODO, to do the calculations is presented.

The strongest influence on the AAF results from the projection of the Debye cone on the cylindrical detector. Since the width of the detector aperture is not zero a curved section of the Debye cone is observed. The projection of this section on the cylindrical detector is in first approximation a parabola. In most discussions of the AAF this parabolic approximation is used. In the case of a shift of the Laue cone's origin along the axis of the sample (*z*-shift), one arm of the parabola is shortened while the other is elongated, resulting in an increased asymmetry. This effect has been discussed in detail in many publications (i.e. Finger et al [1]). In the case of a parallel primary beam, this is sufficient to describe the AAF in terms of sample height and detector height. However, it is not sufficient for the case of a converging beam discussed in this paper.

When axial divergences are considered, Debye cones will be tilted out of the main diffraction plane of the instrument (*â*-tilt). This affects the AAF in a way similar to the *z*-shift. In a geometry with an ideally focussing monochromator all rays of the primary beam hit the sample at the same point, right in the macroscopic diffraction plane. The height of the sample, otherwise an important factor for the asymmetry function, is thus effectively zero and the height of the monochromator becomes the important factor. The resulting AAF is similar, but not identical, to that resulting from the parallel beam model and its dependency on the Bragg diffraction angle is different. Moreover, the shape of the reflections is strongly dependent on the focus length of the monochromator. If the monochromator focuses directly on the sample, the diffraction peaks have very high asymmetry [2]. If the focus is behind the sample, the two effects of *z*-shift and -tilt correlate in a way to cancel out each other. In order for this to be most effective, however, the sample must be high enough. In general this is not the case, thus an increase in sample height would reduce the asymmetry in most instrumental set-ups of this type.

The final AAF is determined by the distribution of the intensity in the two parameter space of sample height and axial divergence angle. For its calculation the respective heights, distances and angles of source, monochromator, sample and detector all have to be considered. Additionally, apertures between source and sample block some of the possible paths, thus changing the intensity distribution. Apertures between sample and detector block parts of the Debye cone only and therefore have to be treated differently from those in front of the sample.

An additional influence on the AAF results from the difference between the macroscopic monochromator diffraction angle 2 and the real diffraction angle 2 $_M$ of the Laue condition. Their relation depends on the tilt angles $_0$ of the primary ray and of the secondary ray as $\cos 2 _M = \cos 2 \cos _0 \cos + \sin _0 \sin$. In a focussing geometry $_0$ and have opposite signs for most rays, resulting in 2 $< 2 _M$.

The program QUASIMODO calculates the peak shape by means of a combination of ray tracing and analytical approach, using ray tracing in front of the sample and an analytical expression for the projection of the Debye cones. The source of rays is modelled as a linear source of limited height with isotropic emission. Each calculated ray is described by its initial height above the macroscopic diffraction plane and by its initial angle with respect to it. The way of the rays are calculated through various slits placed between the source and the monochromator and between the monochromator and the sample, respectively. For those rays hitting the monochromator the reflected ray is calculated according to the Laue equation based on the orientation of the monochromator crystals diffraction vector. Thus the resulting angles and heights *z* for those rays hitting the sample are a result of the initial values at the source and the orientation of the respective monochromator crystal.

For each ray hitting the sample the AAF for a Bragg reflection with a given value of 2 is calculated from the projection of the ray's individual Debye cone on the cylindrical detector; for this the full function is used instead of the parabolic approximation. Shifts due to deviations of 2 from 2 $_M$ are applied after that. The AAF of all rays are added up to give the final AAF of the reflection, which is folded with a Gaussian function in order to include the horizontal broadening. Fitting the parameters of peak width and AAF to an experimental data set is possible. Experimental tests have been done with data measured on E9 at the HMI [3].

[1] Finger, L. W.; Cox, D. E.; Jephcoat, A. P.: J. Appl. Cryst. 27, 892-900 (1994).

[2] Többens, D. M.; Tovar, M.: Applied Physics A, A74, 136-138 (2002).

[3] Többens, D. M. et al.: Mater. Sci. Forum. 378-381, 288-293 (2001).

T13 - P231

NEW EMPIRICAL EXPRESSIONS TO CALCULATE THE TRANSMISSION FACTOR FOR CYLINDRICAL SAMPLES

J. Birkenstock

Universitaet Bremen, FB5-Kristallographie, Klagenfurter Str.2, D-28359 Bremen, Germany.

The calculation of the intensities of reflections in diffraction experiments includes a transmission factor T which is dependent on the geometry of the diffraction experiment. While for the common Bragg Brentano reflecting geometry the transmission factor is assumed to be constant for all angles 2 of diffraction T is a function of 2 for transmission measurements. Among others in [1] and [2] values of T are given for cylindrical samples as a function of discrete and ·R being calculated by numerical integration, where is the samples absorption factor and R the radius of the cylinder. Here, ·R ranges from 0 to 20 in [1] and 0 to 2.5 in [2], with three significant digits in [1] and five in [2]. These values have been used by several authors and also here as reference data to develop simple empirical expressions to calculate T as a function of given and ·R.

The expressions given in [3] have been used in Rietveld programs for many years, though it was explicitly limited to be valid up to ·R 1 which is usually fulfilled for neutron diffraction experiments but often not for x-ray diffraction. This e.g. has been pointed out by [4] who used the following approximating formula to calculate T as a function of and ·R:

$$T \quad A_L \cos^2 \quad A_B \sin^2 \qquad (1)$$

where A_L and A_B are the absorption factors at the Laue and the Bragg condition, i.e. at = 0° and 90°, respectively. A_L and A_B can be calculated by extensive analytical expressions, cited from [5], as a function of ·R. Using (1), the maximum deviations from the tabulated values in [1] are given at = 45°, ranging from 1 % for ·R = 1 to 20 % for ·R = 20. Thus the largest errors occur where the density of reflections is usually rather high.

$$T \quad A \sin^2 \quad B \cos^2 \quad C \sin \ /2 \quad D \cos \ /2 \qquad (2)$$

With this fully empirical approach the coefficients A, B, C and D can no longer be calculated directly and thus have been determined for each tabulated ·R by the least squares method, fitting (2) to the tabulated values. This yielded for each ·R a separate set of A, B, C and D. Fig. 1 displays the coefficients A – D as functions of ·R.

The resulting errors at = 45° between the calculated values and the tabulated ones range from 0.06 % for ·R = 1 to 2.4 % for ·R = 20 and from visual inspection the overall agreement is much better than in [4]. It is noted that a more rigorous comparison could be based on residuals or Chi¸ values, but these are not given in [4]. In contrast to [4] the maximum deviations occur at = 0° ranging from 0.07 % for ·R = 1 over 1.4 % for ·R = 5 and 53 % for ·R = 10 to 325 % for ·R = 20, i.e. being rapidly increasing inaccurate with higher ·R. At the practically more meaningful observation angle of = 5°, though, the deviations are much less being 0.02 % for ·R = 1, 5.9 % for ·R = 5, 9.6 % for ·R = 10 and 11.6 % for ·R = 20, respectively.

Due to the much better overall agreement of (2) with the tabulated values and the fact that the density of reflections at lower angles is usually much less than at intermediate angles (2) is considered to be preferable to (1).

From the coefficients A – D the transmission factor may be computed for any diffraction angle, but only for the discrete values of ·R which are given in [1] and [2]. For intermediate values of ·R interpolated values A – D have to be derived. This is non-trivial in regions where the coefficients are somewhat erratically spread with small changes of ·R. Thus, in a second refinement step, for each coefficient A, B, C and D an individual empirical function was set up to describe it as a function of ·R from which the respective coefficient can be calculated directly for any given ·R. The respective functions are:

$$A \quad R \quad A_A \, e^{\,R/B_A} \quad C_A \quad D_A \quad R \quad E_A \quad R^2 \quad F_A \quad R^3 \qquad (3)$$

with: $A_A = 0.8222(46)$, $B_A = 0.6437(71)$, $C_A = 0.1543(45)$, $D_A = -0.0188(17)$, $E_A = 0.00117(19)$, $F_A = -2.67(59)\cdot10^{-5}$

$$B \quad R \quad A_B \, e^{\,R/B_B} \quad C_B \quad D_B \quad R \quad E_B \quad R^2 \quad F_B \quad R^3 \quad G_B \quad R^4 \quad H_B \quad R^5 \qquad (4)$$

with: $A_B = 1.0454(87)$, $B_B = 0.6695(54)$, $C_B = -0.0537(92)$, $D_B = 0.0509(57)$, $E_B = -0.00968(13)$, $F_B = 0.00084(14)$, $G_B = -3.43(69)\cdot10^{-5}$, $H_B = 5.4(1.2)\cdot10^{-7}$

$$C \quad R \quad A_C \frac{\sqrt{4\ln 2}}{B_C\sqrt{}} e^{\frac{4\ln 2(\ R\ C_C)^2}{B_C^2}} \quad D_C \frac{\sqrt{4\ln 2}}{E_C\sqrt{}} e^{\frac{4\ln 2(\ R\ F_C)^2}{E_C^2}} \quad G_C \frac{\sqrt{4\ln 2}}{H_C\sqrt{}} e^{\frac{4\ln 2(\ R\ I_C)^2}{H_C^2}} \quad (5)$$
$$J_C \quad K_C \quad R \quad L_C \ (\ R)^2 \quad M_C \ (\ R)^5$$

with (n.r. = not refined): A_C = 0.0076(29), B_C =1.60(19), C_C = 2.4142(n.r.), D_C = -0.0368(22), E_C = 1.315(34), F_C = 0.55435(n.r.), G_C =0.0264(33), H_C = 3.34(13), I_C = 3.27(19), J_C = 0.01613(87), K_C = -0.00247(19), L_C = 8.9(1.1)·10^{-5}, M_C = -1.40(47)·10^{-9}

$$D \quad R \quad A_D \frac{\sqrt{4\ln 2}}{B_D\sqrt{}} e^{\frac{4\ln 2(\ R\ C_D)^2}{B_D^2}} \quad D_D \frac{\sqrt{4\ln 2}}{E_D\sqrt{}} e^{\frac{4\ln 2(\ R\ F_D)^2}{E_D^2}} \quad G_D \frac{\sqrt{4\ln 2}}{H_D\sqrt{}} e^{\frac{4\ln 2(\ R\ I_D)^2}{H_D^2}} \quad (6)$$
$$J_D \quad K_D \quad R \quad L_D \ (\ R)^2 \quad M_D \ e^{\ R/N_D}$$

with: A_D = 0.0043(46), B_D = 0.82(30), C_D = 1.932(51), D_D = -0.0215(37), E_D = 0.887(72), F_D = 0.592(21), G_D =0.0198(95), H_D = 1.92(47), I_D =2.73(29), J_D = -0.0589(40), K_D = 0.00274(58), L_D = -4.6(2.0)·10^{-5}, M_D = 0.0665(55), N_D = 1.82(25)

In Fig. 1 the solid lines represent the curves that have been calculated from equations (3) to (6). Thus, in reversed order, for a given ·R the coefficients A – D may be calculated from eqs. (3) – (6) from which T can be calculated for a given by eq. (2). Since the errors of some parameters are rather high compared to the values themselves it was tested if the respective terms could be omitted. But it turned out in all cases that the resulting fit is much worse both from the respective residuals and the graphical inspection. Thus the above formulas represent an operative way to calculate transmission factors for all values of ě·R ranging from 0 to 20.

[1] J.S. Kasper, K. Lonsdale (eds.), *International Tables for X-ray Crystallography, Vol II* (1972), Kluwer Academic Pub., Dordrecht.

[2] A.J.C. Wilson (ed.), *International Tables for Crystallography, Vol C* (1995), Kluwer Academic Pub., Dordrecht

[3] K.D. Rouse, M.J. Cooper, *Acta Cryst.* A26 (1970), 682-691.

[4] T.M. Sabine, B.A. Hunter, W.R. Sabine, C.J. Ball, *J. Appl. Cryst.* 31 (1998), 47-51.[5] C.W. Dwiggins, *Acta Cryst.* A28 (1972), 219-220.

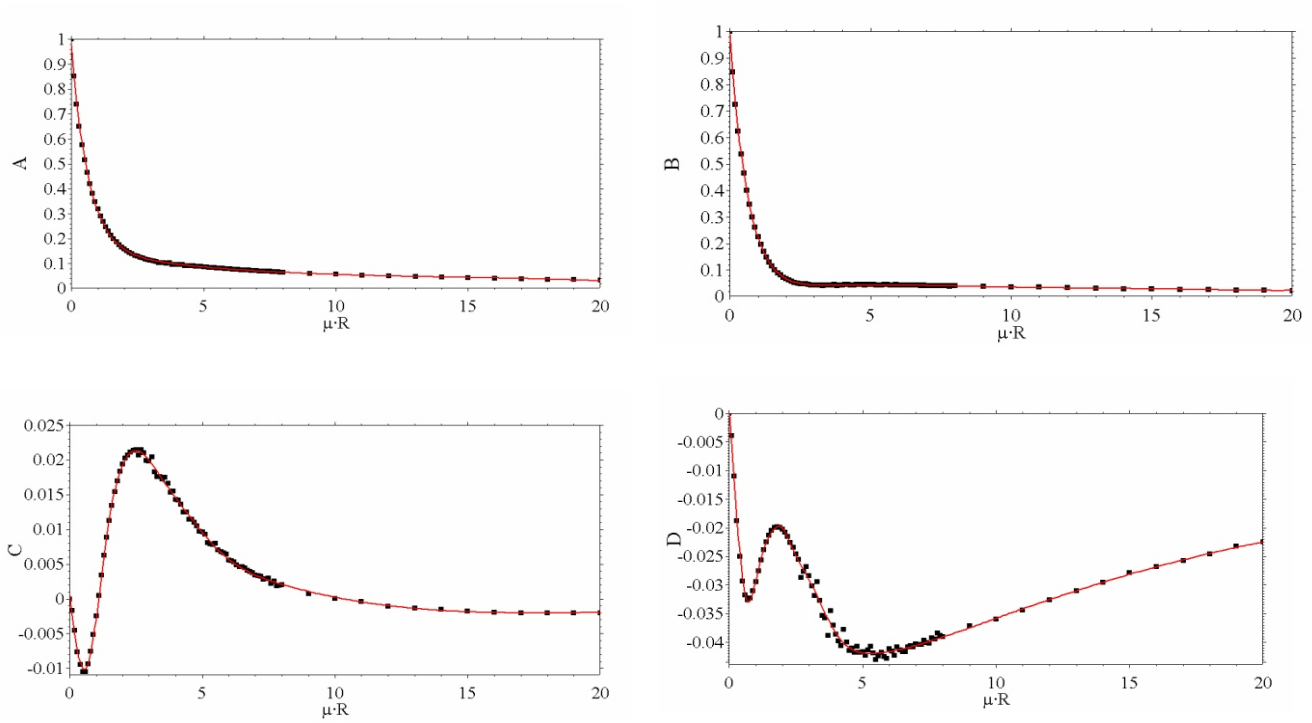

Figure 1: Solid dots are the refined coefficients A, B, C respectively D of eq. (2) as a function ě·R. The solid lines represent empirical curves calculated from equations (3) – (6) obtained by a second refinement.